

# Finite-time predictor line-of-sight-based adaptive neural network path following for unmanned surface vessels with unknown dynamics and input saturation

Yalei Yu<sup>1</sup> , Chen Guo<sup>1,2</sup> and Haomiao Yu<sup>2</sup>

## Abstract

In the presence of unknown dynamics and input saturation, a finite-time predictor line-of-sight-based adaptive neural network scheme is presented for the path following of unmanned surface vessels. The proposed scheme merges with the guidance and the control subsystem of unmanned surface vessels together. A finite-time predictor-based line-of-sight guidance law is developed to ensure unmanned surface vessels effectively converging to and following the referenced path. Then, the path-following control laws are designed by combining neural network-based minimal learning parameter technique with backstepping method, where minimal learning parameter is applied to account for system nonparametric uncertainties. The key features of this scheme, first, the finite-time predictor errors are guaranteed; second, designed controllers are independent of the system model; and third, only required two parameters update online for each control law. The rigorous theory analysis verifies that all signals in the path-following guidance-control system are semi-globally uniformly ultimately bounded via Lyapunov stability theory. Simulation results illustrate the effectiveness and performance of the presented scheme.

## Keywords

Unmanned surface vessels, path following, finite time, line-of-sight, minimal learning parameter, adaptive control

Date received: 26 July 2018; accepted: 30 September 2018

Topic: Robot Manipulation and Control

Topic Editor: Yangquan Chen

Associate Editor: Ning Wang

## Introduction

In the past decades, unmanned surface vessels (USVs) attract ubiquitous attention in rescue, exploration, military, and commerce fields, and its path following problem has been widely investigated.<sup>1–5</sup> High-accuracy path following control acts a pivotal role for an USV to successfully complete its task that reaches and stays a predefined parametric path automatically without time information.<sup>6,7</sup> Actually, path following means the output maneuvering problem that involves geometric and dynamic tasks of an USV's closed-loop system, where the former task can be solved by a guidance law for steering and the latter task needs a kinetics controller such that it satisfies desired dynamic behaviors.<sup>8,9</sup>

It is interesting that line-of-sight (LOS) guidance law is an effective algorithm that has been extensively studied from a couple of different perspectives, and various strategies have been developed to obtain higher tracking performance.<sup>2,3,5–7,9–13</sup> On the one hand, the traditional LOS guidance law has been modified by proposing a time-varying

<sup>1</sup>The School of Navigation, Dalian Maritime University, Dalian, China

<sup>2</sup>The School of Marine Electrical Engineering, Dalian Maritime University, Dalian, China

### Corresponding author:

Chen Guo, The School of Marine Electrical Engineering and The School of Navigation, Dalian Maritime University, Dalian 116026, China.

Email: dmuguoc@126.com



Creative Commons CC BY: This article is distributed under the terms of the Creative Commons Attribution 4.0 License

(<http://www.creativecommons.org/licenses/by/4.0/>) which permits any use, reproduction and distribution of the work without further permission provided the original work is attributed as specified on the SAGE and Open Access pages (<https://us.sagepub.com/en-us/nam/open-access-at-sage>).

look-ahead distance combining with a so-called integral LOS (ILOS) to compensate for the drift force by adding the integral action.<sup>10</sup> From this point of view, Fossen et al. further extended the ILOS and proposed adaptive LOS (ALOS) that provided integral action by adding adaptive law for sideslip angle.<sup>9</sup> On the other hand, considering the disturbances induced by ocean currents that were expressed by virtue of relative velocities, the direct and indirect adaptive methods were used to deal with this condition.<sup>11</sup> In previous studies,<sup>2,13</sup> two guidance laws, extended state observer (ESO)-based LOS (ELOS) and predictor-based LOS (PLOS), were presented. They are different from the directly estimated sideslip angle, which are based on ESO and predictor-based position errors to estimate it indirectly. However, it should be noticed that all these achievements, by adding integral action to compensate for the sideslip angle, merely focus on the topic of kinematic level (geometric task), whereas the kinetic level (dynamic task or velocity requirement) have not been mentioned and assumed that along-tracking error is always zero.<sup>8,9,11</sup> And then these controllers simply chose the proportion–integral–derivative (PID) or the common sliding-mode based on Nomoto's model.

Therefore, a solution to these aforementioned problems was proposed by Zheng and Sun,<sup>12</sup> which can be used in various parametric paths and still works when disturbed by the time-varying ocean currents. In fact, sideslip angle may be large in practical appliances, whereas the aforementioned references only satisfy the state of steady navigation of the USV with small sideslip angle.<sup>2,9,10,13</sup> Hence, it will lose stability in the presence of significant external disturbances.<sup>14</sup> In this context, Ning Wang et al. developed a finite-time sideslip observer to exactly estimate time-varying large sideslip angle in a short time.<sup>7</sup> Along this line of consideration, an extended result was presented by Miao et al.<sup>5</sup> and wherein a compound line-of-sight (CLOS) method was developed to handle the situation that sideslip angles are produced by relative sway velocity and ocean currents separately and can still work when the former relative sideslip angle is approximately more than  $20^\circ$ . All these aforementioned guidance laws cannot ensure the stability of the guidance signals in a finite time except the one proposed by Wang et al.<sup>7</sup> In the study by Jin,<sup>15</sup> a finite-time convergence of LOS was solved by time-varying tan-type barrier Lyapunov functions. In addition, from the prospective of designing a finite-time controller, a global finite-time stable controller was illustrated by PID sliding mode control (PID-SMC) algorithm presented by Yan et al.<sup>16</sup> Furthermore, finite-time observer-based tracking control was presented by Wang et al.<sup>17</sup> Unfortunately, this controller was for unmanned underwater vehicles. To achieve higher path-following performance, sliding mode, reinforcement learning, and object recognition approaches have been extensively studied.<sup>3,18–21</sup>

Regarding the problem of system nonparametric uncertainties, it is a common phenomenon in an industrial control environment.<sup>22</sup> Fortunately, universal function approximator was developed to estimate the unknown system dynamics caused

by nonparametric uncertainties via neural networks (NNs) or fuzzy systems, owing to their learning and adaptation abilities.<sup>23</sup> In this case, there are many research achievements,<sup>12,22,24–28</sup> which show NNs sufficient performance on approximating nonlinear dynamics. In aforementioned statements, a common weakness of these NN-based control approaches is that the approximator depends on the number of the NN nodes. The online update parameters will grow significantly with increasing NN nodes. As for the question just mentioned, an alternative method is estimating the norm of the ideal weighting vector replacing the elements of the weighting vector.<sup>29–33</sup> This idea also has been applied to fuzzy system in previous studies.<sup>34,35</sup> In this context, a deep-rooted information adaptive approach was presented by Song et al.<sup>36</sup> Moreover, an alternatively effective approach for uncertain system and unknown dynamics is an adaptive approximation-based regulation control combining with a single-hidden-layer feed-forward network proposed by Wang et al.<sup>37</sup> Due to the physical characters of actuator, however, these methods satisfied necessarily the input saturation constraint, which is the another limitation discussed in the following.

The input saturation constraint is induced by physical limitations, generally, almost every actuator is suffered from saturation and subjected to magnitude and rate constraints.<sup>12,23</sup> Moreover, saturation can influence the system performance severely, such as lag, overshoot, and instability.<sup>12</sup> The approaches to handle this problem were proposed in previous studies.<sup>38–43</sup> An auxiliary design system was introduced to compensate for the input saturation of underactuated or full-actuated ships in previous studies<sup>38–40,42</sup> and in Harmouche et al.'s study<sup>43</sup> for global tracking control was investigated. In addition, in the presence of input saturation, autonomous underwater vehicles and aircrafts also have been studied.<sup>41,44</sup>

Motivated by the above observations and with an effort to address previous questions, the finite-time predictor line-of-sight–based adaptive neural network (FPANN) scheme is presented for path following of USVs in the presence of unknown dynamics and input saturation. The main contributions of this article are summarized as follows:

1. A novel finite-time predictor–based line-of-sight (FPLOS) guidance law is presented for the path following problem of USVs. Comparing with the PLOS guidance law proposed by Liu et al.,<sup>13</sup> the finite-time convergence of the predictor errors are guaranteed by the proposed FPLOS with faster transient and stable performance.
2. In this article, all the parameters of the system are unknown. The effective controllers are developed by only approximate partly unknown dynamics including virtual control by minimal learning parameter, in the absence of coefficient for the unknown dynamics. These unknown coefficients are avoided by designing suitable Lyapunov function.
3. An auxiliary design system is introduced to compensate for the input saturation constraint. Moreover, the

kinematic and kinetic levels are considered together with FPANN scheme using FPLOS guidance laws, MLP, and backstepping techniques.

The rest of this article is organized as follows. The second section states the problem formulation. Guidance-control system design is presented in the third section, devoting to design guidance-control algorithms of USVs. The stability analysis of the entire closed-loop system presented in the fourth section. The fifth section provides simulation results. The sixth section concludes this article.

**Define 1.** The following notations are used in this article. For a scalar  $a \in \mathbb{R}_+$  denotes  $a > 0$ .  $\mathbb{R}^m$  is the  $m$ -dimensional Euclidean space.  $(\cdot)^T$  denotes the transpose of a matrix  $(\cdot)$ .  $\|\cdot\|$  represents the Euclidean norm and  $\|\cdot\|^2 = \sum_{i,j} \{ \cdot \}_{i,j}^2$ .  $(\cdot)_{i,j}$  denotes the element of  $(\cdot)$  in row  $i$  and column  $j$ .  $|\cdot|$  represents the absolute value of a scalar.  $(\hat{\cdot})$  denotes the estimated value, and  $(\tilde{\cdot})$  describes the error of approximation.  $(\cdot)_{\max}$  represents the maximum value.

## Problem formulation

This section states USV's model, assumptions, lemmas, radial basis function neural network (RBFNN), and control objective, which will be used in the controllers design and stability analysis later.

### USVs' model

The mathematical model of an USV on a horizontal plane, including its kinematics and dynamics, is described as follows<sup>1,39</sup>

$$\begin{cases} \dot{x} = u \cos(\psi) - v \sin(\psi) \\ \dot{y} = u \sin(\psi) + v \cos(\psi) \\ \dot{\psi} = r \end{cases} \quad (1)$$

$$\begin{cases} \dot{u} = \frac{1}{m_{11}} \left( \underbrace{m_{22}vr - d_{11}u - \sum_{i=2}^3 d_{ui}|u|^{i-1}u}_{f_u(\cdot)} \right) + \frac{1}{m_{11}} \tau_u + \frac{1}{m_{11}} \delta_{d,u} \\ \dot{v} = \frac{1}{m_{22}} \left( \underbrace{m_{11}ur - d_{22}v - \sum_{i=2}^3 d_{vi}|v|^{i-1}v}_{f_v(\cdot)} \right) + \frac{1}{m_{22}} \delta_{d,v} \\ \dot{r} = \frac{1}{m_{33}} \left( \underbrace{(m_{11} - m_{22})uv - d_{33}r - \sum_{i=2}^3 d_{ri}|r|^{i-1}r}_{f_r(\cdot)} \right) + \frac{1}{m_{33}} \tau_r + \frac{1}{m_{33}} \delta_{d,r} \end{cases} \quad (2)$$

where  $[x, y, \psi]^T$  denotes the position  $(x, y)$  and the attitude  $\psi$  of the USV in the earth-fixed frame. The vector  $[u, v, r]^T$  describes the surge velocity  $u$ , the sway velocity  $v$ , and yaw rate  $r$  of the USV in the body-fixed frame. The terms  $m_{11}, m_{22}$ , and  $m_{33}$  denote the USV inertia mass, including added mass. The terms  $d_{11}, d_{22}, d_{33}$  and  $d_{ij} (i = u, v, r), (j = 2, 3)$  are hydrodynamic damping in surge, sway, and yaw. The vector  $[\tau_u, 0, \tau_r]^T$  contains the surge force  $\tau_u$  and yaw moment  $\tau_r$ . The vector  $[\delta_{d,u}, \delta_{d,v}, \delta_{d,r}]^T$  represents the external disturbances caused by waves, wind, and ocean currents. Noting that the inertia mass and hydrodynamic damping are unknown. In this article, the external disturbances are out of the scope of this investigation.

### RBFNN

The RBFNN can approximate any continuous function  $f_{nn}(\bar{x}) : \mathbb{R}^m \rightarrow \mathbb{R}$  over the compact set  $\mathcal{Q}_{\bar{x}} \in \mathbb{R}^m$  to any arbitrary accuracy by setting numerous hidden neurons<sup>45</sup>

$$f_{nn}(\bar{x}) = \mathbf{W}^{*T} \mathbf{\Theta}(\bar{x}) + \kappa \quad (3)$$

where the input vector  $\bar{x} \in \mathcal{Q}_{\bar{x}}$ .  $\mathbf{W}^*(t) = [w_1, w_2, \dots, w_l] \in \mathbb{R}^l$  represents the ideal weight vector. It is worth mentioning that  $\mathbf{W}^*$  is only quantities required for analytical purpose.

In practical applications, its estimations  $\hat{\mathbf{W}}$  are used for the function approximation and then the estimation of  $f_{nn}(\bar{x})$ <sup>46</sup>

$$\hat{f}_{nn}(\bar{x}) = \hat{\mathbf{W}}^T \mathbf{\Theta}(\bar{x}) \quad (4)$$

where  $\mathbf{\Theta}(\bar{x}) = [\theta_1(\bar{x}), \dots, \theta_l(\bar{x})]^T$  is a vector of radial basis function vector, the element of which is given by

$$\theta_j(\bar{x}) = a_j \exp \left( -\frac{\|\bar{x} - \mathbf{b}_j\|^2}{2c_j^2} \right), (j = 1, \dots, l) \quad (5)$$

where  $a_j$  is the gain coefficient,  $\mathbf{b}_j = [b_{j1}, b_{j2}, \dots, b_{jm}]^T \in \mathbb{R}^m$  is the center of the receptive field, and  $c_j$  is the spread of Gaussian function. The approximation error  $\kappa$  is bounded by unknown positive constant  $\bar{\kappa}$  over a compact set  $\mathcal{Q}_{\bar{x}}$ , namely,  $0 < |\kappa| < \bar{\kappa} < \infty$ . For the sake of simplicity, according to minimal-learning parameter method was appeared in previous studies.<sup>30,33</sup> Define  $\phi = \|\mathbf{W}\|^2$  and then the  $\hat{\phi}$  is used to estimate the optimal weight.

### Assumptions

**Assumption 1.** The vector  $[u, v, r]^T$  is measurable.

**Assumption 2.** The unknown sideslip angle  $\beta$  is bounded and slowly time-varying, satisfying  $\dot{\beta} \approx 0$ .

**Assumption 3.** The desired heading angle  $\psi_d$  can be precisely tracked by the actual heading  $\psi$  such that  $\psi = \psi_d$ .

**Assumption 4.** The optimal weight value is bounded, satisfying  $|\phi_i| \leq \phi_{i\max}$ , ( $i = u, r$ ), where  $\phi_{i\max}$  is a positive constant.

**Assumption 5.** The control inputs  $\tau_i$ , ( $i = u, r$ ) is determined by the saturated function of the control command  $\tau_{i0}$  as follows

$$\tau_i = \text{sat}(\tau_{i0}) = \begin{cases} \tau_{im}, & \text{if } \tau_{i0} > \tau_{im} \\ \tau_{i0}, & \text{if } -\tau_{im} \leq \tau_{i0} \leq \tau_{im} \\ -\tau_{im}, & \text{if } \tau_{i0} < -\tau_{im} \end{cases} \quad (6)$$

where  $\tau_{im}$ , ( $i = u, r$ ) is the magnitude constraints of the surge force and yaw moment, respectively.

**Remark 1.** In Assumption 1, the measurable states are reasonable assumption.<sup>22</sup> Otherwise, observers are needed to estimate the unknown dynamics.<sup>47</sup> Assumption 2 is a reasonable assumption,<sup>1,9</sup> and the sideslip angle  $\beta$  is quite small,<sup>10</sup> satisfying  $\beta \approx \sin\beta$ . According to Assumption 3, one has  $\psi - \gamma_p = \psi_d - \gamma_p$ , where  $\gamma_p$  will be mentioned later. This is a common assumption in the LOS-based guidance scheme.<sup>2,3,7,9,10,13</sup> The way to relax the assumption was mentioned in previous works.<sup>2,9</sup> Assumption 4 is also reasonable and appeared in previous studies.<sup>12,22,28,47</sup> In addition, one should be observed that the USV system<sup>2</sup> is underactuated, thus it tracks a path with arbitrarily large curvature impossibly. It is necessary to adopt regular and smooth path.<sup>48</sup> Assumption 5 is set according to practical applications.<sup>12,38</sup>

### Lemmas

**Lemma 1<sup>49</sup>.** For  $(x, y) \in \mathbb{R}^2$ , the following Young's inequality holds

$$xy \leq \frac{\varepsilon^p}{p} |x|^p + \frac{1}{q\varepsilon^q} |y|^q \quad (7)$$

where  $\varepsilon$  is a positive constant, and the constants  $p > 1, q > 1$ , satisfying  $(p-1)(q-1) = 1$ .

**Lemma 2<sup>50</sup>.** Suppose  $(a, b) \in \mathbb{R}_+^2$  and  $0 < \nu < 1$ , the following inequality holds

$$(a+b)^\nu \leq a^\nu + b^\nu \quad (8)$$

$$\sqrt{ab} \leq \sqrt{a} + \sqrt{b}. \quad (9)$$

**Lemma 3<sup>12</sup>.** The following switching function  $h(\mathbf{x}) : \mathbb{R}^n \rightarrow \mathbb{R}$  is an  $n$ th-order smooth nonlinear function

$$h(\mathbf{x}) = \begin{cases} 0, & \|\mathbf{x}\| \leq \chi_a \\ 1 - \cos^n \left( \frac{\pi}{2} \sin^n \left( \frac{\pi \|\mathbf{x}\|^2 - a^2}{b^2 - a^2} \right) \right), & \chi_a < \|\mathbf{x}\| \\ 1, & \|\mathbf{x}\| \leq \chi_b \end{cases} \quad (10)$$

**Lemma 4<sup>51,52</sup>.** Consider system  $\dot{\mathbf{x}} = f(\mathbf{x})$ ,  $f(\mathbf{x}) = \mathbf{0}$ ,  $\mathbf{x} \in \mathbb{R}^n$ , where  $f(\cdot) : \mathbb{R}^n \rightarrow \mathbb{R}^n$  is a continuous function. One assumes that there is a continuous positive differentiable

function  $V(\mathbf{x}) : U \rightarrow \mathbb{R}$ , which satisfies the following differential inequality in an open neighborhood  $U_0 \subset U$  of the origin such that

$$V(\mathbf{0}) = 0, V(\mathbf{x}) > 0, \forall \mathbf{x} \neq \mathbf{0} \quad (11)$$

$$V(\mathbf{x}) \leq -\alpha V^\rho(\mathbf{x}), \mathbf{x} \in U_0 \setminus \{\mathbf{0}\} \quad (12)$$

where  $V(\mathbf{x}) = 0$  be an equilibrium point and  $\alpha \in \mathbb{R}_+, 0 < \rho < 1$ . Then, the origin is a finite-time stable equilibrium of system  $\dot{\mathbf{x}} = f(\mathbf{x})$  and the finite settling time  $T_f$  can be given by  $T_f(x_0) \leq \frac{V(x_0)^{(1-\rho)}}{\alpha(1-\rho)}$ . If  $U = \mathbb{R}^n$  and  $V$  are radially unbounded, the origin is a globally finite-time stable equilibrium.

**Lemma 5<sup>13,53</sup>.** Let  $\mathbf{x} = \mathbf{0}$  be an equilibrium point of  $\dot{\mathbf{x}} = f(\mathbf{x}, t)$  and assumed that  $f$  is locally Lipschitz in  $\mathbf{x}$  uniformly in  $t$ . Let  $V : [0, \infty) \times \mathbb{R}^n \rightarrow \mathbb{R}$  be a continuously differentiable, positive, and radially unbounded function  $V(\mathbf{x})$  such that

$$\dot{V} = \frac{\partial V}{\partial \mathbf{x}} f(\mathbf{x}, t) \leq -K(\mathbf{x}) \leq 0, \forall t \geq 0, \forall \mathbf{x} \in \mathbb{R}^n \quad (13)$$

where  $K$  is a continuous function. Then, all solutions of  $\dot{\mathbf{x}} = f(\mathbf{x}, t)$  are uniformly bounded and satisfy  $\lim_{t \rightarrow \infty} K(\mathbf{x}(t)) = 0$ . In addition, if  $K(\mathbf{x})$  is positive definite, then the equilibrium  $\mathbf{x} = \mathbf{0}$  is uniformly asymptotical stable (UAS).

### Control objective

Design control laws  $\tau$  and the update law  $\dot{\theta}$  of the path variable  $\theta$  of the virtual point along a prescribed path  $\eta_p(\theta) \in \mathbb{R}^q$  with  $q \geq 1$  parameterized by  $(x_p(\theta), y_p(\theta))$  under the conditions represented by Assumptions 1 to 5, such that the position and velocity tracking errors of the USV converge to an arbitrarily small neighborhood of zero within a short time, that is,  $\sup_{t \in [t_0, \infty]} \|x - x_p\| \leq \varepsilon_x$ ,

$\sup_{t \in [t_0, \infty]} \|y - y_p\| \leq \varepsilon_y$ , and  $\sup_{t \in [t_0, \infty]} \|u - u_d\| \leq \varepsilon_u$ , where  $\varepsilon_x, \varepsilon_y$  and  $\varepsilon_u$  are small positive constants, and  $u_d$  denotes the desired surge velocity designed later; see Figure 1.

### Guidance-control system design

In this section, as shown in Figure 2, one develops FPLOS guidance law and control algorithms, where latter is designed by combining with MLP and backstepping techniques.

#### FPLOS guidance

In this subsection, the FPLOS guidance scheme is designed to compensate for sideslip angle. Since drift force significantly affects USVs tracking performance and even

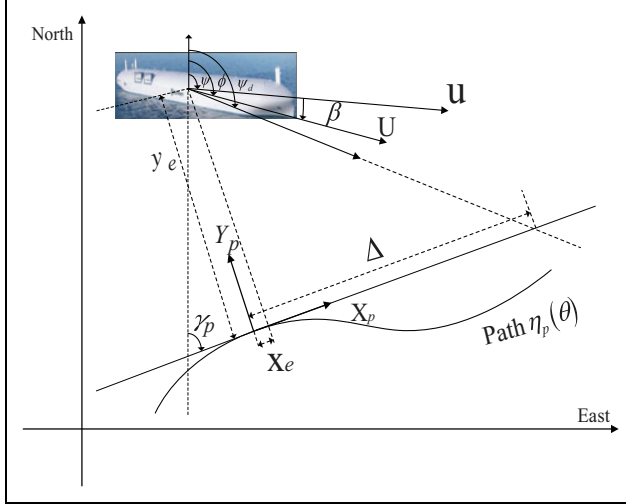


**Figure 1.** Geometrical illustration of path-following control.

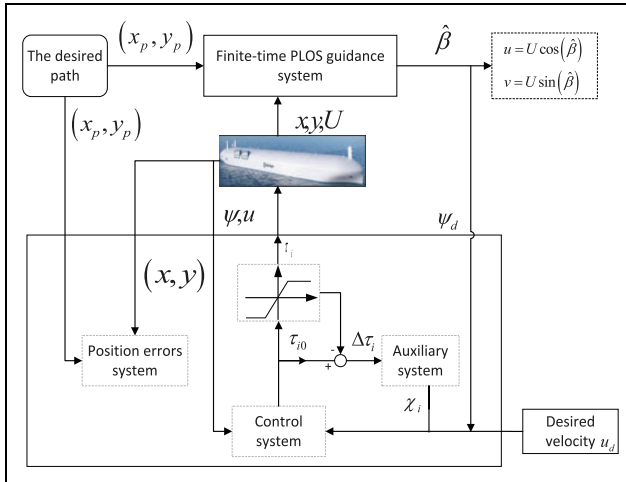


**Figure 2.** Control schematic of USVs. USV: unmanned surface vessel.

deteriorates it, if the sideslip angle produced by drift force is not properly compensated.<sup>1-3,5,7,9,10,12,13</sup>

**Path following error dynamics.** The path-normal line from the point  $(x_p(\theta), y_p(\theta))$  through the USV located at the point  $(x, y)$  defines the along- and cross-tracking error variables  $(x_e, y_e)$ . One now interprets the position errors to the path-tangential reference frame as

$$\begin{bmatrix} x_e \\ y_e \end{bmatrix} = \begin{bmatrix} \cos(\gamma_p) & -\sin(\gamma_p) \\ \sin(\gamma_p) & \cos(\gamma_p) \end{bmatrix}^T \begin{bmatrix} x - x_p \\ y - y_p \end{bmatrix} \quad (14)$$

where  $\gamma_p$  denotes the path-tangential angle given by  $\gamma_p = \text{atan2}(y'_p(\theta), x'_p(\theta)) \in [-\pi, \pi]$ . By differentiating  $x_e$  and  $y_e$  with respect to time in combination with Assumption 3, we have

$$\begin{cases} \dot{x}_e = U \cos(\psi - \gamma_p) - U \sin(\psi - \gamma_p)\beta \\ \quad + y_e \dot{\gamma}_p - u_{tot} \\ \dot{y}_e = U \sin(\psi - \gamma_p) + U \cos(\psi - \gamma_p)\beta - x_e \dot{\gamma}_p \end{cases} \quad (15)$$

where  $U = \sqrt{u^2 + v^2}$ ,  $0 < U_{\min} \leq U \leq U_{\max}$ . The term  $\beta = \text{atan2}(v, u)$  describes the sideslip angle, and  $u_{tot} = \dot{\theta} \sqrt{y_p'^2(\theta) + x_p'^2(\theta)}$  represents the total speed of the virtual reference point moving along the curved path.

**Estimation sideslip angle.** To estimate the unknown sideslip angle  $\beta$ , according to equation (15), one proposes two predictors as follows

$$\begin{cases} \dot{\hat{x}}_e = U \cos(\psi - \gamma_p) - U \sin(\psi - \gamma_p)\hat{\beta} \\ \quad + \hat{y}_e \dot{\gamma}_p - u_{tot} - k_x \text{sig}^\rho(\tilde{x}_e) \\ \dot{\hat{y}}_e = U \sin(\psi - \gamma_p) + U \cos(\psi - \gamma_p)\hat{\beta} \\ \quad - \hat{x}_e \dot{\gamma}_p - k_y \text{sig}^\rho(\tilde{y}_e) \end{cases} \quad (16)$$

where  $\tilde{x}_e = \hat{x}_e - x_e$  and  $\tilde{y}_e = \hat{y}_e - y_e$  are prediction errors. The coefficients  $k_x$  and  $k_y$  are positive constants. And  $\hat{\beta}$  is the estimation of  $\beta$ . The term  $\text{sig}^\rho(\tilde{e}) = |\tilde{e}|^\rho \text{sign}(\tilde{e})$  where  $\tilde{e} = \{\tilde{x}_e, \tilde{y}_e\}$  and  $0 < \rho < 1$ . Therefore, the update law for  $\hat{\beta}$  can be designed as follows

$$\begin{aligned} \dot{\hat{\beta}} &= k_1 [U \sin(\psi - \gamma_p) \tilde{x}_e - U \cos(\psi - \gamma_p) \tilde{y}_e] \\ &\quad - k_1 k_2 \text{sig}^\rho(\tilde{\beta}) \end{aligned} \quad (17)$$

where  $(k_1, k_2) \in \mathbb{R}_+^2$ ,  $\text{sig}^\rho(\tilde{\beta}) = |\tilde{\beta}|^\rho \text{sign}(\tilde{\beta})$ .

Consequently, by combining with equations (15) to (17) and Assumption 3, results can be obtained as follows

$$\begin{cases} \dot{\tilde{x}}_e = -U \sin(\psi - \gamma_p) \tilde{\beta} + \tilde{y}_e \dot{\gamma}_p - k_x \text{sig}^\rho(\tilde{x}_e) \\ \dot{\tilde{y}}_e = U \cos(\psi - \gamma_p) \tilde{\beta} - \tilde{x}_e \dot{\gamma}_p - k_y \text{sig}^\rho(\tilde{y}_e) \\ \dot{\tilde{\beta}} = k_1 [U \sin(\psi - \gamma_p) \tilde{x}_e - U \cos(\psi - \gamma_p) \tilde{y}_e] \\ \quad - k_1 k_2 \text{sig}^\rho(\tilde{\beta}) \end{cases} \quad (18)$$

**Remark 2.** The error system in equation (18) is significantly different from the error system provided by Liu Lu et al.<sup>13</sup> First of all, one introduces the fractional power terms  $\text{sig}^\rho(\cdot)$  among error signal dynamics  $\tilde{x}_e, \tilde{y}_e$  and  $\tilde{\beta}$ .<sup>50</sup> Secondly, we add two compulsory terms  $\tilde{y}_e \dot{\gamma}_p$  and  $(-\tilde{x}_e \dot{\gamma}_p)$  into  $\tilde{x}_e$  and  $\tilde{y}_e$ , respectively, according to equations (15) and (16).

**Theorem 1.** Considering that the presented update law  $\dot{\hat{\beta}}$  given by equation (17) renders the predictor errors  $\tilde{x}_e$  and  $\tilde{y}_e$  to converge to origin within a finite time and the system (equation (18)) is UAS.

**Proof.** Choosing the following Lyapunov function candidate (LFC)  $V_1 = \frac{1}{2} \tilde{x}_e^2 + \frac{1}{2} \tilde{y}_e^2 + \frac{1}{2} \tilde{\beta}^2$ , the time differentiation of  $V_1$  can be obtained as follows

$$\begin{aligned}
\dot{V}_1 &= \tilde{x}_e \left( -U \sin(\psi - \gamma_p) \tilde{\beta} + \tilde{y}_e \dot{\gamma}_p - k_x \text{sig}^\rho(\tilde{x}_e) \right) \\
&\quad + \tilde{y}_e \left( U \cos(\psi - \gamma_p) \tilde{\beta} - \tilde{x}_e \dot{\gamma}_p - k_y \text{sig}^\rho(\tilde{y}_e) \right) \\
&\quad + \tilde{\beta} [U \sin(\psi - \gamma_p) \tilde{x}_e - U \cos(\psi - \gamma_p) \tilde{y}_e - k_2 \text{sig}^\rho(\tilde{\beta})] \\
&= -k_x \tilde{x}_e \text{sig}^\rho(\tilde{x}_e) - k_y \tilde{y}_e \text{sig}^\rho(\tilde{y}_e) - k_2 \tilde{\beta} \text{sig}^\rho(\tilde{\beta}) \\
&\leq -k_x |\tilde{x}_e|^{\rho+1} - k_y |\tilde{y}_e|^{\rho+1} - k_2 |\tilde{\beta}|^{\rho+1} \\
&= -k_x (\tilde{x}_e^2)^{\frac{\rho+1}{2}} - k_y (\tilde{y}_e^2)^{\frac{\rho+1}{2}} - k_2 (\tilde{\beta}^2)^{\frac{\rho+1}{2}} \\
&\leq -k \left( (\tilde{x}_e^2)^{\frac{\rho+1}{2}} + (\tilde{y}_e^2)^{\frac{\rho+1}{2}} + (\tilde{\beta}^2)^{\frac{\rho+1}{2}} \right)
\end{aligned} \tag{19}$$

where  $k = \min\{k_x, k_y, k_2\}$ .

Using Lemma 1, we have

$$\begin{aligned}
\dot{V}_1 &\leq -k (\tilde{x}_e^2 + \tilde{y}_e^2 + \tilde{\beta}^2)^{\frac{\rho+1}{2}} \\
&\leq -2^{\frac{\rho+1}{2}} k V_1
\end{aligned} \tag{20}$$

Hence, according to Lemma 3, the predictor errors  $(\tilde{x}_e, \tilde{y}_e)$  can be rendered to the origin  $(0, 0)$  in a finite time, and the setting time  $T_1$  satisfies  $T_1 \leq \frac{2V(y(0))^{\frac{1-\rho}{2}}}{2^{\frac{\rho+1}{2}} k (1-\rho)}$ . By Lemma 4, we have the system equation (16) is UAS. This completes the proof.

**The FPLOS guidance law.** The augmented FPLOS guidance heading is designed as follows

$$\psi_d = \gamma_p + \arctan \left( -\frac{\hat{y}_e + \Delta \hat{\beta}}{\Delta} \right) \tag{21}$$

where  $0 < \Delta_{\min} \leq \Delta \leq \Delta_{\max}$  is specified look-ahead distance defined by users. From the first equation of (15), the velocity  $u_{\text{tot}}$  can be recognized as a virtual control to stabilize  $\hat{x}_e$ . Hence,  $u_{\text{tot}}$  is provided as follows

$$u_{\text{tot}} = k_3 \hat{x}_e + U \cos(\psi - \gamma_p) - U \sin(\psi - \gamma_p) \hat{\beta} \tag{22}$$

where  $k_3$  is a positive constant. The update law of the path variable  $\theta$  is chosen as follows

$$\dot{\theta} = \frac{k_3 \hat{x}_e + U \cos(\psi - \gamma_p) - U \sin(\psi - \gamma_p) \hat{\beta}}{\sqrt{\dot{x}_p^2 + \dot{y}_p^2}} \tag{23}$$

**Theorem 2.** Applying the FPLOS guidance laws (21) to (23) to the path-following kinematic subsystem (equation (15)), and one can obtain along- and cross-tracking errors system equation (16) which is UAS.

**Proof.** Substituting the FPLOS guidance laws (21) to (23) into the path-following errors system equation (16), we obtain

$$\begin{cases} \dot{\hat{x}}_e = -k_3 \hat{x}_e + \hat{y}_e \dot{\gamma}_p - k_x \text{sig}^\rho(\tilde{x}_e) \\ \dot{\hat{y}}_e = -\frac{U \hat{y}_e}{\sqrt{\Delta^2 + (\hat{y}_e + \Delta \hat{\beta})^2}} - \hat{x}_e \dot{\gamma}_p - k_y \text{sig}^\rho(\tilde{y}_e) \end{cases} \tag{24}$$

Employing LFC  $V_\theta = \frac{1}{2} \hat{x}_e^2 + \frac{1}{2} \hat{y}_e^2$ . Taking the time derivative of  $V_\theta$  along equation (24) results in

$$\begin{aligned}
\dot{V}_\theta &= -k_3 \hat{x}_e^2 - \omega \hat{y}_e^2 - k_x \hat{x}_e \text{sig}^\rho(\tilde{x}_e) - k_y \hat{y}_e \text{sig}^\rho(\tilde{y}_e) \\
&\leq -k_3 \hat{x}_e^2 - \omega \hat{y}_e^2 - k_x \hat{x}_e |\tilde{x}_e|^\rho - k_y \hat{y}_e |\tilde{y}_e|^\rho
\end{aligned} \tag{25}$$

where  $\omega = \left( \frac{U}{\sqrt{\Delta^2 + (\hat{y}_e + \Delta \hat{\beta})^2}} \right)_{\min}$

Using the fact that it derived from Young's inequality as follows

$$\begin{cases} \hat{x}_e |\tilde{x}_e|^\rho \leq \frac{1}{2} \hat{x}_e^2 + \frac{1}{2} (|\tilde{x}_e|^\rho)^2 \\ \hat{y}_e |\tilde{y}_e|^\rho \leq \frac{1}{2} \hat{y}_e^2 + \frac{1}{2} (|\tilde{y}_e|^\rho)^2 \end{cases} \tag{26}$$

Substituting equation (26) into (25) yields

$$\begin{aligned}
\dot{V}_\theta &\leq -\left(k_3 - \frac{k_x}{2}\right) \hat{x}_e^2 - \left(\omega - \frac{k_y}{2}\right) \hat{y}_e^2 \\
&\quad + \frac{k_x}{2} (|\tilde{x}_e|^\rho)^2 + \frac{k_y}{2} (|\tilde{y}_e|^\rho)^2 \\
&\leq -\varpi V_\theta + \frac{k_x}{2} |\tilde{x}_e|^{2\rho} + \frac{k_y}{2} |\tilde{y}_e|^{2\rho}
\end{aligned} \tag{27}$$

where  $\varpi = \min\{k_3 - \frac{k_x}{2}, \omega - \frac{k_y}{2}\} > 0$ . By Theorem1, one has  $(\tilde{x}_e, \tilde{y}_e) = (0, 0), \forall t > T_1$ . It follows that  $\dot{V}_\theta \leq -\varpi V_\theta$  holds for all  $t > T_1$ . By Lemma4, we have the system equation (16) is UAS. This concludes the proof.

## Control design

In this subsection, designing the control laws  $\tau_u$  and  $\tau_r$  force the USV to reach and stay at the desired path  $\eta_p(\theta)$ . Define the attitude tracking error variables  $\psi_e = \psi - \psi_d, u_e = u - \alpha_u$  and  $r_e = r - \alpha_r$ , where  $\alpha_r$  and  $\alpha_u$  are virtual control laws designed as follows

$$\begin{cases} \alpha_u = u_d \\ \alpha_r = -k_\psi \psi_e + \dot{\psi}_d \end{cases} \tag{28}$$

where  $u_d$  is the desired surge velocity and  $k_\psi$  is a positive constant. The objective of designing virtual control law realizes  $\lim_{t \rightarrow \infty} U \rightarrow U_d$ ,<sup>28</sup> where  $U_d$  denotes desired velocity (velocity size). Combining with the fact that  $U = \sqrt{u^2 + v^2}$ , it is easy to see  $u \rightarrow u_d = \sqrt{U_d^2 - v^2}, \forall U_d \geq |v|$ .

The time-derivative of errors  $u_e$  and  $r_e$  along equations (2) and (28) results can be obtained as follows

$$\begin{cases} \dot{u}_e = \frac{1}{m_{11}}f_u(\cdot) + \frac{1}{m_{11}}\tau_u - \dot{\alpha}_u \\ \dot{r}_e = \frac{1}{m_{33}}f_r(\cdot) + \frac{1}{m_{33}}\tau_r - \dot{\alpha}_r \end{cases} \quad (29)$$

The above equations can be simplified as follows

$$\begin{cases} \dot{u}_e = \frac{1}{m_{11}} \underbrace{(f_u(\cdot) - m_{11}\dot{\alpha}_u)}_{g_u(\cdot)} + \frac{1}{m_{11}}\tau_u \\ \dot{r}_e = \frac{1}{m_{33}} \underbrace{(f_r(\cdot) - m_{33}\dot{\alpha}_r)}_{g_r(\cdot)} + \frac{1}{m_{33}}\tau_r \end{cases} \quad (30)$$

By introducing the MLP to approximate the lumpily unknown dynamic in system equation (30), we have

$$\begin{cases} \hat{g}_u = k_{nu}u_e\hat{\phi}_u\Theta^T(\mathbf{v})\Theta(\mathbf{v}) \\ \hat{g}_r = k_{nr}r_e\hat{\phi}_r\Theta^T(\mathbf{v})\Theta(\mathbf{v}) \end{cases} \quad (31)$$

where  $(k_{nu}, k_{nr}) \in \mathbb{R}_+^2$ .

Considering input saturation, the corresponding nominal control laws are designed as follows

$$\begin{cases} \tau_{u0} = -k_{nu}u_e\hat{\phi}_u\Theta^T(\mathbf{v})\Theta(\mathbf{v}) - k_{u0}u_e + k_{u0}\chi_u \\ \tau_{r0} = -k_{nr}r_e\hat{\phi}_r\Theta^T(\mathbf{v})\Theta(\mathbf{v}) - \psi_e - k_{r0}r_e + k_{r0}\chi_r \end{cases} \quad (32)$$

where  $(k_u, k_r, k_{u0}, k_{r0}) \in \mathbb{R}_+^4$ .

For the facility of constraint effect analysis of the input saturation, the auxiliary system is given by

$$\begin{cases} \dot{\chi}_u = -k_{\chi u}\chi_u - \frac{|u_e\Delta\tau_u| + 0.5\rho_u^2\Delta\tau_u^2}{\chi_u}h(\chi_u) + \rho_u\Delta\tau_u \\ \dot{\chi}_r = -k_{\chi r}\chi_r - \frac{|r_e\Delta\tau_r| + 0.5\rho_r^2\Delta\tau_r^2}{\chi_r}h(\chi_r) + \rho_r\Delta\tau_r \end{cases} \quad (33)$$

where  $(k_{\chi u}, k_{\chi r}, \rho_u, \rho_r) \in \mathbb{R}_+^4$ . In addition,  $\Delta\tau_u = \tau_u - \tau_{u0}$  and  $\Delta\tau_r = \tau_r - \tau_{r0}$ .

The update laws of MLP RBFNN are designed as follows

$$\begin{cases} \dot{\hat{\phi}}_u = \Gamma_u(k_{nu}u_e^2\Theta^T(\mathbf{v})\Theta(\mathbf{v}) - \vartheta_u\hat{\phi}_u) \\ \dot{\hat{\phi}}_r = \Gamma_r(k_{nr}r_e^2\Theta^T(\mathbf{v})\Theta(\mathbf{v}) - \vartheta_r\hat{\phi}_r) \end{cases} \quad (34)$$

where  $(\Gamma_u, \Gamma_r, \vartheta_u, \vartheta_r) \in \mathbb{R}_+^4$ .

**Remark 3.** In fact, the USV in question is no actuation in the sway dynamic. The sway velocity, however, is bounded, and the conclusion will be proven later. Hence, the approximation of sway dynamic is omitted. The readers are interested in the approximation of sway dynamic; see Zheng et al. and Wang et al.'s studies.<sup>6,7</sup>

## Stability analysis

**Theorem 3.** Consider the USV is described by equation (2), satisfying Assumptions 1 to 5, the guidance laws (21) to (23), the control laws (32) with adaptive laws (34), and auxiliary system equation (33) are applied to it. Then initial conditions are bounded and satisfy  $\boldsymbol{\eta}_1^T(\mathbf{0})\boldsymbol{\eta}_1(\mathbf{0}) + \mathbf{z}^T(\mathbf{0})\mathbf{z}(\mathbf{0}) + \tilde{\boldsymbol{\Phi}}^T(\mathbf{0})\tilde{\boldsymbol{\Phi}}(\mathbf{0}) \leq V_{\max}$ , where  $\boldsymbol{\eta}_1 = [\hat{x}_e, \hat{y}_e, \psi_e]^T$ ,  $\mathbf{z} = [u_e, r_e]^T$  and  $\boldsymbol{\Phi} = [\tilde{\phi}_u, \tilde{\phi}_r]^T$  is a positive definite matrix. Hence, one can tune the positive design parameters  $k_1, k_2, k_3, k_x, k_y, k_\psi, k_u, k_r, k_{u0}, k_{r0}, k_{nu}, k_{nr}, k_{\chi u}, k_{\chi r}, \lambda_u, \lambda_r, \rho_u, \rho_r, \vartheta_u, \vartheta_r, \Gamma_u$ , and  $\Gamma_r$  such that error signals  $\mathbf{z}$ ,  $\boldsymbol{\eta}_1$ , and  $\boldsymbol{\Phi}$  are SGUUB. Moreover, the vector  $\mathbf{N} = [\hat{x}_e, \hat{y}_e, \psi_e, u_e, r_e, \tilde{\phi}_u, \tilde{\phi}_r]$  remains the level set  $\mathcal{Q}_1 := \{V \leq \frac{\gamma_v}{2\varsigma_v}\}$ , where  $\gamma_v$  and  $\varsigma_v$  will be designed later.

**Proof.** Consider the following complete LFC  $V = V_\theta + \frac{1}{2}\psi_e^2 + \frac{1}{2}m_{11}u_e^2 + \frac{1}{2}m_{33}r_e^2 + \frac{1}{2}\chi_u^2 + \frac{1}{2}\chi_r^2 + \frac{1}{2\Gamma_u}\tilde{\phi}_u^2 + \frac{1}{2\Gamma_r}\tilde{\phi}_r^2$ . Differentiating  $V$  in virtue of equations (27) and (30) to (34) with respect to time for all  $t > T_1$ , one yields

$$\begin{aligned} \dot{V} \leq & -\left(k_u - \frac{k_x}{2}\right)\hat{x}_e^2 - \left(\omega - \frac{k_y}{2}\right)\hat{y}_e^2 - k_\psi\psi_e^2 \\ & + \psi_e r_e + u_e \left(k_{nu}u_e\hat{\phi}_u\Theta^T(\mathbf{v})\Theta(\mathbf{v}) + \kappa_u + \tau_u\right) \\ & + r_e \left(k_{nr}r_e\hat{\phi}_r\Theta^T(\mathbf{v})\Theta(\mathbf{v}) + \kappa_r + \tau_r\right) \\ & + \chi_u\dot{\chi}_u + \chi_r\dot{\chi}_r - \frac{1}{\Gamma_u}\tilde{\phi}_u\dot{\hat{\phi}}_u - \frac{1}{\Gamma_r}\tilde{\phi}_r\dot{\hat{\phi}}_r \end{aligned} \quad (35)$$

According to Lemma 1, it is worth noticing that the following inequalities hold

$$u_e\kappa_u \leq \frac{1}{2}u_e^2 + \frac{1}{2}\kappa_u^2 \quad (36)$$

$$r_e\kappa_r \leq \frac{1}{2}r_e^2 + \frac{1}{2}\kappa_r^2 \quad (37)$$

$$k_{u0}\chi_u u_e \leq \frac{k_{u0}}{2}\chi_u^2 + \frac{k_{u0}}{2}u_e^2 \quad (38)$$

$$k_{r0}\chi_r r_e \leq \frac{k_{r0}}{2}\chi_r^2 + \frac{k_{r0}}{2}r_e^2 \quad (39)$$

$$\rho_u\Delta\tau_u\chi_u \leq \frac{1}{2}\rho_u^2\Delta\tau_u^2 + \frac{1}{2}\chi_u^2 \quad (40)$$

$$\rho_r\Delta\tau_r\chi_r \leq \frac{1}{2}\rho_r^2\Delta\tau_r^2 + \frac{1}{2}\chi_r^2 \quad (41)$$

$$\begin{aligned} \vartheta_u\tilde{\phi}_u\hat{\phi}_u &= \vartheta_u\tilde{\phi}_u(\phi_u - \tilde{\phi}_u) \\ &\leq \frac{\vartheta_u}{2}\phi_{u\max}^2 - \frac{\vartheta_u}{2}\tilde{\phi}_u^2 \end{aligned} \quad (42)$$

$$\begin{aligned} \vartheta_r\tilde{\phi}_r\hat{\phi}_r &= \vartheta_r\tilde{\phi}_r(\phi_r - \tilde{\phi}_r) \\ &\leq \frac{\vartheta_r}{2}\phi_{r\max}^2 - \frac{\vartheta_r}{2}\tilde{\phi}_r^2 \end{aligned} \quad (43)$$

Substituting equations (36) to (43) into equation (35) yields

$$\begin{aligned}
\dot{V} \leq & -\left(k_u - \frac{k_x}{2}\right)\hat{x}_e^2 - \left(\omega - \frac{k_y}{2}\right)\hat{y}_e^2 - k_\psi \psi_e^2 \\
& -\left(k_u - \frac{k_{u0}}{2} - \frac{1}{2}\right)u_e^2 - \left(k_r - \frac{k_{r0}}{2} - \frac{1}{2}\right)r_e^2 \\
& -\left(k_{\chi u} - \frac{k_{u0}}{2} - \frac{1}{2}\right)\chi_u^2 - \left(k_{\chi r} - \frac{k_{r0}}{2} - \frac{1}{2}\right)\chi_r^2 \\
& -\frac{1}{2}\rho_u^2 \Delta\tau_u^2 (h(\chi_u) - 1) - \frac{1}{2}\rho_r^2 \Delta\tau_r^2 (h(\chi_r) - 1) \\
& +\frac{1}{2}\kappa_u^2 + \frac{1}{2}\vartheta_u \phi_{u\max}^2 + \frac{1}{2}\kappa_r^2 + \frac{1}{2}\vartheta_r \phi_{r\max}^2 \\
& -|u_e \Delta\tau_u| \left(h(\chi_u) - \text{sgn}(u_e \Delta\tau_u)\right) \\
& -|r_e \Delta\tau_r| \left(h(\chi_r) - \text{sgn}(r_e \Delta\tau_r)\right) \\
& -\frac{\vartheta_u}{2}\tilde{\phi}_u^2 - \frac{\vartheta_r}{2}\tilde{\phi}_r^2
\end{aligned} \tag{44}$$

For  $h(\chi_i) = 1, (i = u, r)$ , the time-derivative  $V$  reduces to

$$\begin{aligned}
\dot{V} \leq & -\left(k_u - \frac{k_x}{2}\right)\hat{x}_e^2 - \left(\omega - \frac{k_y}{2}\right)\hat{y}_e^2 - k_\psi \psi_e^2 \\
& -\left(k_u - \frac{k_{u0}}{2} - \frac{1}{2}\right)u_e^2 - \left(k_r - \frac{k_{r0}}{2} - \frac{1}{2}\right)r_e^2 \\
& -\left(k_{\chi u} - \frac{k_{u0}}{2} - \frac{1}{2}\right)\chi_u^2 - \left(k_{\chi r} - \frac{k_{r0}}{2} - \frac{1}{2}\right)\chi_r^2 \\
& -\frac{\vartheta_u}{2}\tilde{\phi}_u^2 - \frac{\vartheta_r}{2}\tilde{\phi}_r^2 + \mathcal{V}_1 \\
\leq & -\varsigma_{v1}V + \mathcal{V}_1
\end{aligned} \tag{45}$$

where  $\varsigma_{v1} = \min\{k_3 - \frac{k_x}{2}, \omega - \frac{k_y}{2}, k_\psi, k_u - \frac{k_{u0}}{2} - \frac{1}{2}, k_r - \frac{k_{r0}}{2} - \frac{1}{2}, k_{\chi u} - \frac{k_{u0}}{2} - \frac{1}{2}, k_{\chi r} - \frac{k_{r0}}{2} - \frac{1}{2}, \frac{\vartheta_u}{2}, \frac{\vartheta_r}{2}\}$ , and  $\mathcal{V}_1 = \frac{1}{2}\kappa_u^2 + \frac{1}{2}\vartheta_u \phi_{u\max}^2 + \frac{1}{2}\kappa_r^2 + \frac{1}{2}\vartheta_r \phi_{r\max}^2$

Otherwise, for  $h(\chi_i) < 1$ , similarly, noting the following fact

$$u_e \Delta\tau_u \leq \frac{1}{2}u_e^2 + \frac{1}{2}\Delta\tau_u^2 \tag{46}$$

$$r_e \Delta\tau_r \leq \frac{1}{2}r_e^2 + \frac{1}{2}\Delta\tau_r^2 \tag{47}$$

we have

$$\begin{aligned}
\dot{V} \leq & -\left(k_u - \frac{k_x}{2}\right)\hat{x}_e^2 - \left(\omega - \frac{k_y}{2}\right)\hat{y}_e^2 - k_\psi \psi_e^2 \\
& -\left(k_u - \frac{k_{u0}}{2} - 1\right)u_e^2 - \left(k_r - \frac{k_{r0}}{2} - 1\right)r_e^2 \\
& -\left(k_{\chi u} - \frac{k_{u0}}{2} - \frac{1}{2}\right)\chi_u^2 - \left(k_{\chi r} - \frac{k_{r0}}{2} - \frac{1}{2}\right)\chi_r^2 \\
& +\left(\frac{1}{2} + \frac{\rho_u^2}{2}\right)\Delta\tau_u^2 + \left(\frac{1}{2} + \frac{\rho_r^2}{2}\right)\Delta\tau_r^2 \\
& -\frac{\vartheta_u}{2}\tilde{\phi}_u^2 - \frac{\vartheta_r}{2}\tilde{\phi}_r^2 + \mathcal{V}_2 \\
\leq & -\varsigma_{v2}V + \mathcal{V}_2
\end{aligned} \tag{48}$$

where  $\varsigma_{v2} = \min\{k_3 - \frac{k_x}{2}, \omega - \frac{k_y}{2}, k_\psi, k_u - \frac{k_{u0}}{2} - 1, k_r - \frac{k_{r0}}{2} - 1, k_{\chi u} - \frac{k_{u0}}{2} - \frac{1}{2}, k_{\chi r} - \frac{k_{r0}}{2} - \frac{1}{2}, \frac{\vartheta_u}{2}, \frac{\vartheta_r}{2}\}$ , and  $\mathcal{V}_2 = \frac{1}{2}\kappa_u^2 + \frac{1}{2}\vartheta_u \phi_{u\max}^2 + \frac{1}{2}\kappa_r^2 + \frac{1}{2}\vartheta_r \phi_{r\max}^2 + \left(\frac{1}{2} + \frac{\rho_u^2}{2}\right)\Delta\tau_u^2 + \left(\frac{1}{2} + \frac{\rho_r^2}{2}\right)\Delta\tau_r^2$ .

Combining with equations (45) and (48), the results can be obtained as follows

$$\dot{V} \leq -\varsigma_v V + \mathcal{V}_v \tag{49}$$

where  $\varsigma_v = \min\{\varsigma_{v1}, \varsigma_{v2}\}$  and  $\mathcal{V}_v = \max\{\mathcal{V}_1, \mathcal{V}_2\}$  and design parameter satisfying  $k_u > \frac{k_{u0}}{2} + 1, k_r > \frac{k_{r0}}{2} + 1, k_{\chi u} > \frac{k_{u0}}{2} + \frac{1}{2}$  and  $k_{\chi r} > \frac{k_{r0}}{2} + \frac{1}{2}$

Thus,  $\dot{V}$  is strictly negative outside the set  $\mathcal{Q}_1 = \{V \leq \frac{\mathcal{V}_v}{\varsigma_v}\}$  and follows from equation (49) that

$$V \leq \left(V(0) - \frac{\mathcal{V}_v}{\varsigma_v}\right)e^{-\varsigma_v t} + \frac{\mathcal{V}_v}{\varsigma_v} \tag{50}$$

According to a standard Lyapunov theory extension,<sup>54</sup> the bounded error signals were proved, the tracking errors  $\eta_1$ , the weight approximation errors  $\Phi$ , and velocity errors  $\mathbf{z}$ , respectively. This theorem is a completed proof.

**The sway dynamic.** From the equation (2), the sway dynamic as

$$\dot{v} = \frac{1}{m_{22}} \left( m_{11}ur - d_{22}v - \sum_{i=2}^3 d_{vi}|v|^{i-1}v \right) + \frac{1}{m_{22}}\delta_{d,v} \tag{51}$$

In this note, the external disturbances are out of the scope of this research, assuming USVs in the absence of disturbance, that is,  $\delta_{d,v} = 0$ . In this situation, the sway dynamic can be rewritten by



$$\dot{v} = -\frac{d_{22}}{m_{22}}v + \underbrace{\frac{1}{m_{22}}(m_{11}ur - \sum_{i=2}^3 d_{vi}|v|^{i-1}v)}_{h(v)} \quad (52)$$

By employing Bellman–Gronwall comparison principle,<sup>55</sup> the results can be obtained as follows

$$\begin{aligned} v(t) &\leq v(t_0) e^{-\frac{d_{22}}{m_{22}}(t-t_0)} + \frac{h(v)m_{22}}{d_{22}} \left[ 1 - e^{-\frac{d_{22}}{m_{22}}(t-t_0)} \right] \\ &\leq v(t_0) + \frac{m_{22}}{d_{22}}h(v), \forall t_0 \leq t < \infty. \end{aligned} \quad (53)$$

It can be seen from the above inequality (equation (53)) that the sway dynamics  $v$  is being bounded by combining with the fact that  $r$ ,  $u$ , and  $h(v) < \infty$  are bounded. The similar proof can be seen in previous studies.<sup>6,7,22</sup>

**Remark 4.** In practices, the rudder speed is limited by the physical characters of actuator. Furthermore, the study by Van Amerongen<sup>56</sup> has pointed out that common values of rudder speed are  $\dot{\delta}_{\max} = 2 \sim 7^\circ \text{ deg s}^{-1}$ . Hence, the yaw rate  $|r|$  is bounded. An approach for dealing with state constraints was presented by Hermosilla et al.<sup>57</sup>

**Remark 5.** The closed-loop system only satisfies SGUUB since the RBFNN is introduced in equation (31) can not keep well approximated capability out of the suitable compact set  $\mathcal{Q}_0$ .<sup>22</sup> On the other hand, it can achieve global uniformly ultimately bounded by adding robust control; see the work by Zheng and Sun.<sup>12</sup>

**Remark 6.** The optimal design parameters can be found by gradually decreasing or increasing and testing the simulation runs simultaneously. Furthermore, in this article, the closed-loop controller is divided into two parts between FPLOS-based backstepping controller with auxiliary system and FPLOS-based MLP controller. After adjusting design parameters until they can be taken effect, separately, these two controllers are consolidated together into the presented FPANN controller. And then the optimal parameters are found by changing design parameters slightly.

## Numerical simulation

To illustrate the effectiveness and performance of the presented FPANN scheme, we conduct simulation studies with an USV whose dynamic is given by equations (1) and (2) and its parameters can be found in the work by Lefeber et al.<sup>58</sup> The maximum magnitude of surge force is approximately 0.9 N, and the maximum moment is approximately 0.9 Nm in the work by Lefeber et al.<sup>58</sup> Although in this condition of saturated constraint, the desired surge velocity is increased from 0.05 m s<sup>-1</sup> in the work by Lefeber et al.<sup>58</sup> to 0.3 m s<sup>-1</sup> in this note. Set the look-ahead distance  $\Delta$

**Table 1.** Design parameters of controller.

Notation	Value	Notation	Value	Notation	Value
$k_1$	1	$k_{u0}$	5	$\rho_u$	1
$k_2$	0.1	$k_{r0}$	2	$\rho_r$	1
$k_3$	3	$k_{nu}$	0.5	$\vartheta_u$	0.2
$k_x$	0.3	$k_{nr}$	0.5	$\vartheta_r$	0.04
$k_y$	0.3	$k_{xu}$	2	$l$	25
$k_\psi$	10	$k_{xr}$	2	$c$	0.2
$k_u$	1	$a_u$	1.3	$\rho$	0.6
$k_r$	2	$a_r$	1.9	$\Gamma_u$	1
$\chi_a$	0.1	$\chi_b$	1	$\Gamma_r$	0.8

equal to 1.1. The initial conditions of the USV are given by  $[x(0), y(0), \psi(0)]^T = [0, 1, \frac{\pi}{3}]^T$ ,  $[u(0), v(0), r(0)]^T = [0.3, 0, 0]^T$ . The design parameters are listed in Table 1. The initial values for  $W_u$  and  $W_r$  are selected randomly in the interval (0, 1). The input vectors  $m = 3$  and the centers  $b$  placed in

$$\begin{aligned} (|u|, |v|, |r|) &\in [0 \text{ m s}^{-1}, 5 \text{ m s}^{-1}], [0 \text{ m s}^{-1}, 1.5 \text{ m s}^{-1}], \\ &[0 \text{ rad s}^{-1}, 1.2 \text{ rad s}^{-1}) \end{aligned} \quad (54)$$

The desired path is given by

$$\begin{cases} x_p(\theta) = 10 \sin(0.1\theta) + \theta \\ y_p(\theta) = 10\theta \end{cases} \quad (55)$$

## Case 1

In this simulation, to prove the effectiveness of the proposed FPLOS guidance laws, a comparison analysis is conducted between the FPANN scheme and the PLOS-based adaptive neural network (PANN) scheme in the same design parameters. The comparative results are plotted in Figures 3 to 10 demonstrate that the FPANN provides improved and fast performance. It can be observed that the estimation errors  $(\tilde{x}_e, \tilde{y}_e, \tilde{\beta})$  converge to zero in a finite time, by contrast, these errors of the PANN scheme exhibit slight fluctuating behavior at the beginning period. The heading angle error and update law of parametric path are depicted in Figures 5 and 6, where the heading angle has an obvious oscillation around the steady state with PANN. In addition, the estimated performance of the MLP approximator is shown in Figures 7 and 8, from which we can see that the FPANN scheme supplies fast and accurate approximation of the unknown dynamics. Then, Figure 9 describes the auxiliary system states, herein the state  $\chi_r$  perform a remarkable oscillation both two methods. In Figure 10, it demonstrated that the input saturation problem is effectively compensated by both the FPANN scheme and the PANN scheme, whereas the presented FPANN performs better in transient state.

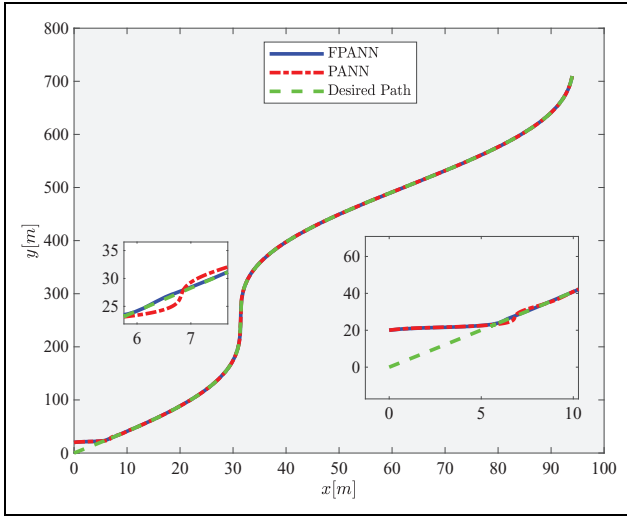


**Figure 3.** The path following performance.

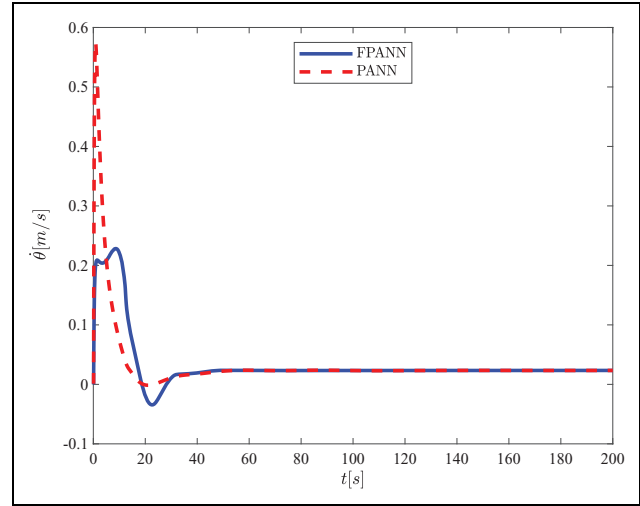


**Figure 6.** The update law of the path variable  $\theta$ .

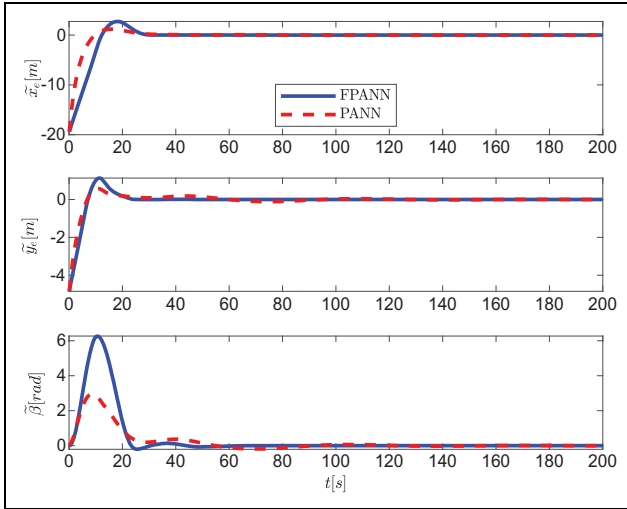


**Figure 4.** The estimation errors of  $\tilde{x}_e$ ,  $\tilde{y}_e$  and  $\tilde{\beta}$ .

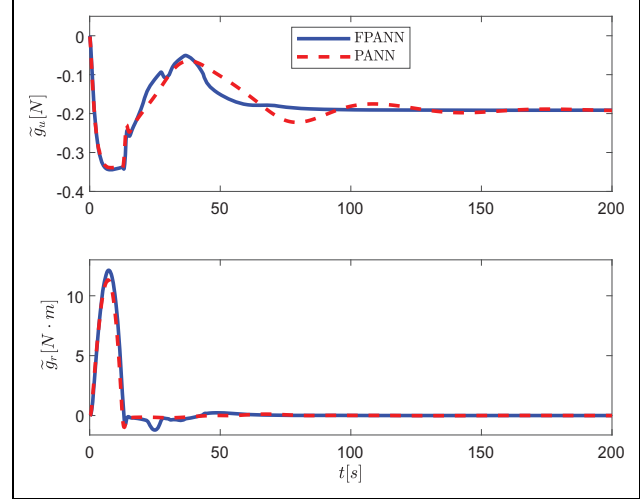


**Figure 7.** The approximation errors of unknown dynamics  $\tilde{g}_u$  and  $\tilde{g}_r$ .

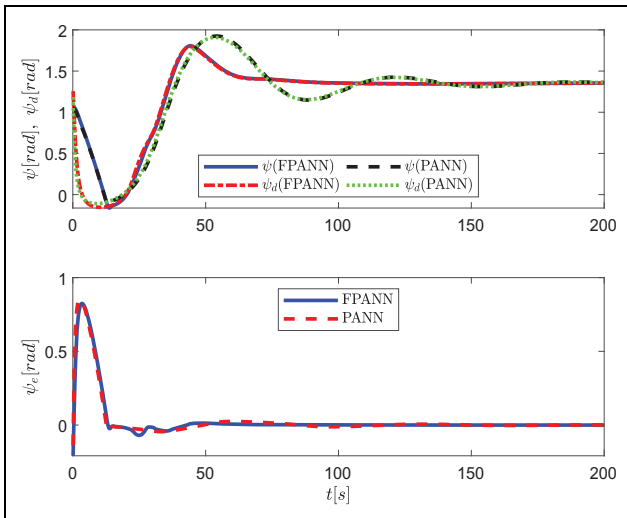


**Figure 5.** The heading angle  $\psi$ , guidance law  $\psi_d$ , and heading error  $\psi_e$ .

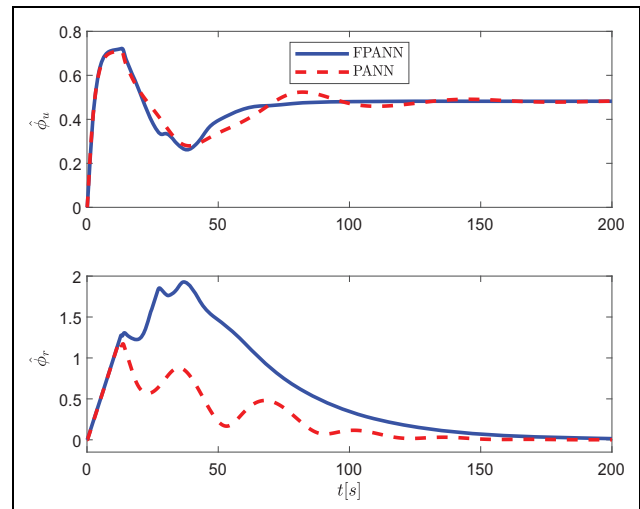


**Figure 8.** The norms of  $\hat{\phi}_u$  and  $\hat{\phi}_r$ .

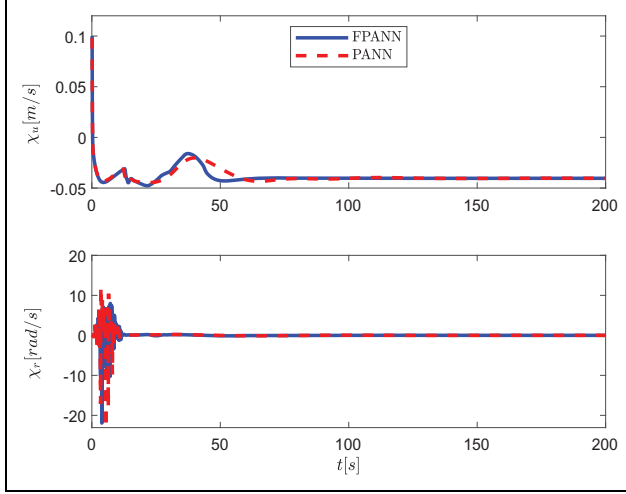


**Figure 9.** The auxiliary system states  $\chi_u$  and  $\chi_r$ .

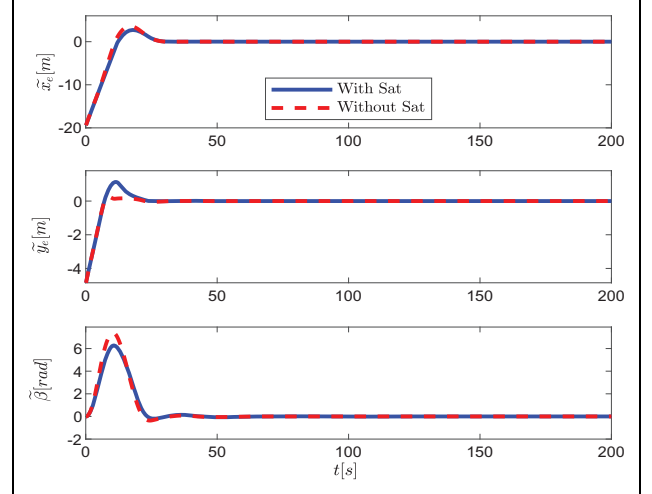


**Figure 12.** The estimation errors of  $\tilde{x}_e$ ,  $\tilde{y}_e$  and  $\tilde{\beta}$ .

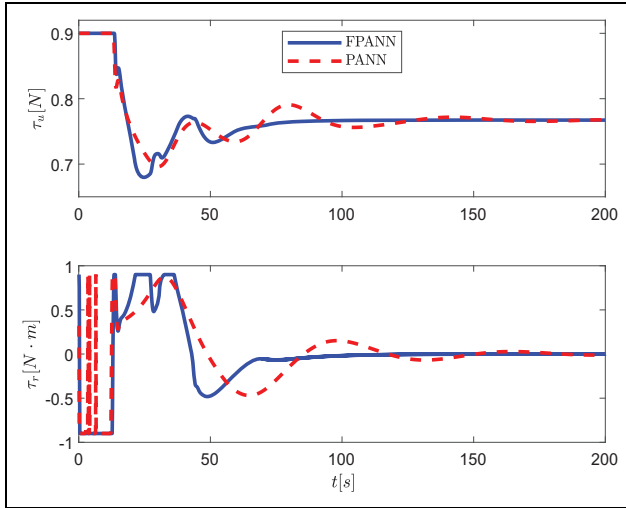


**Figure 10.** The control laws  $\tau_u$  and  $\tau_r$ .

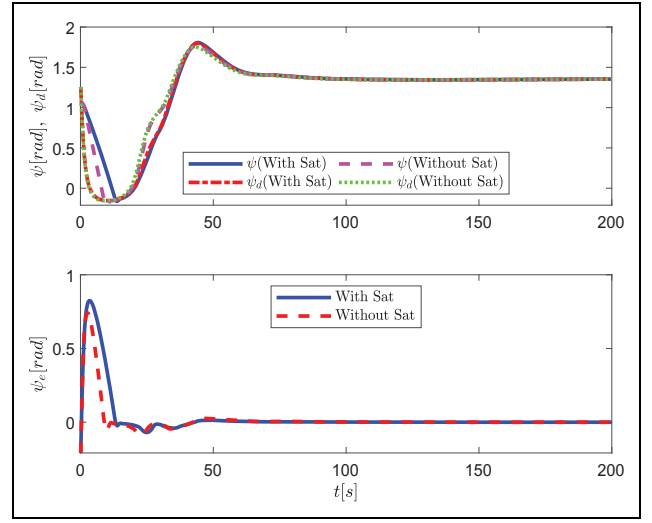


**Figure 13.** The heading angle  $\psi$ , guidance law  $\psi_d$  and heading error  $\psi_e$ .

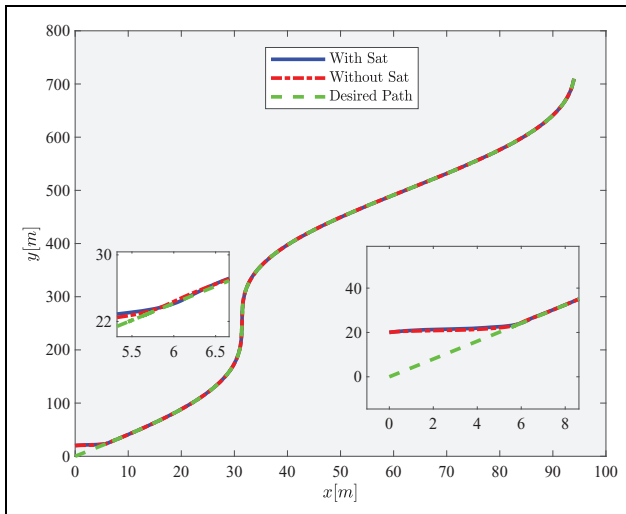


**Figure 11.** The path following performance.

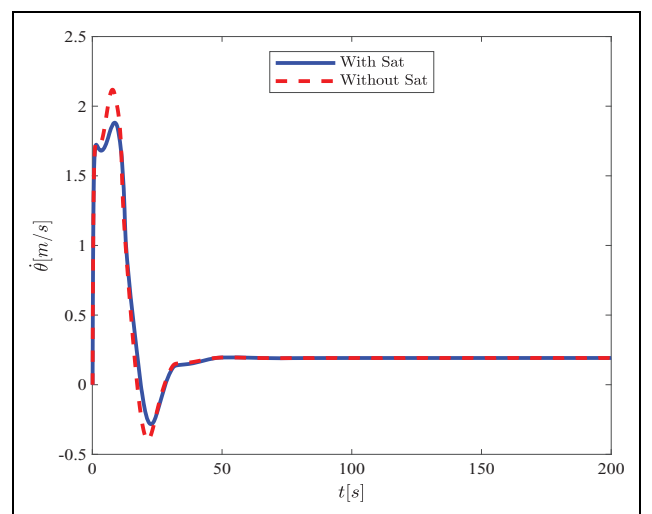


**Figure 14.** The update law of the path variable  $\theta$ .

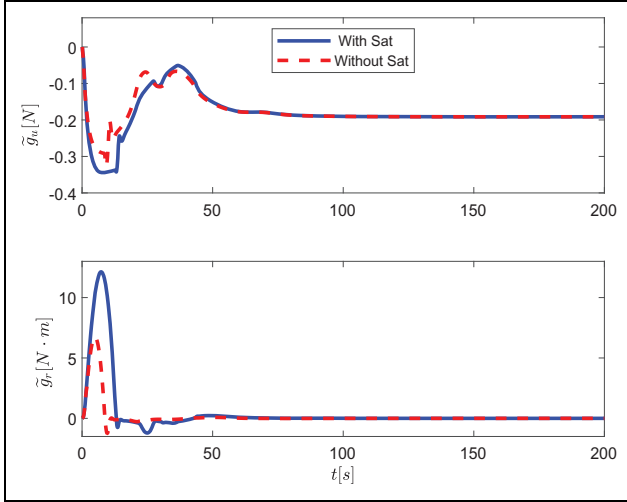


**Figure 15.** The approximation errors of unknown dynamics  $g_u$  and  $g_r$ .

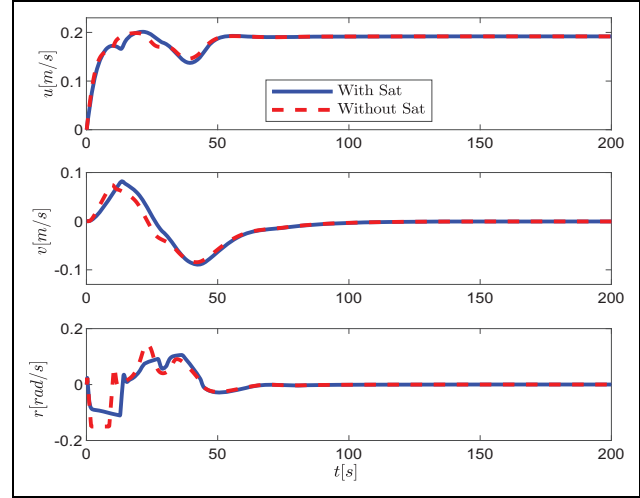


**Figure 17.** The system states  $u$ ,  $v$  and  $r$ .

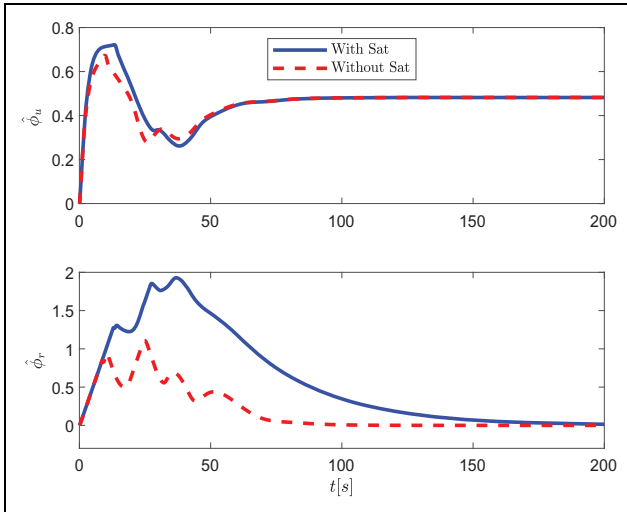


**Figure 16.** The norms of  $\hat{\phi}_u$  and  $\hat{\phi}_r$ .

## Case 2

Similar to the comparison of case 1, another comparison analysis is executed to verify the effective anti-windup performance of the presented FPANN scheme. The controller considering input saturation constraint is marked as With Sat, and the controller without considering input saturation constraint is marked as Without Sat. The results are shown in Figures 11 to 18 that illustrate the presented scheme works effectively and satisfy required conditions of input saturation while the real control inputs beyond the constraint conditions without anti-windup strategies. Figure 11 describes almost the same precise path-following performance even in the presence of input saturation. The error sideslip angle has a small range oscillatory behavior which is shown in Figure 12 with both conditions. The heading angle error converges to an arbitrarily small neighborhood of zero within a short time can be seen from

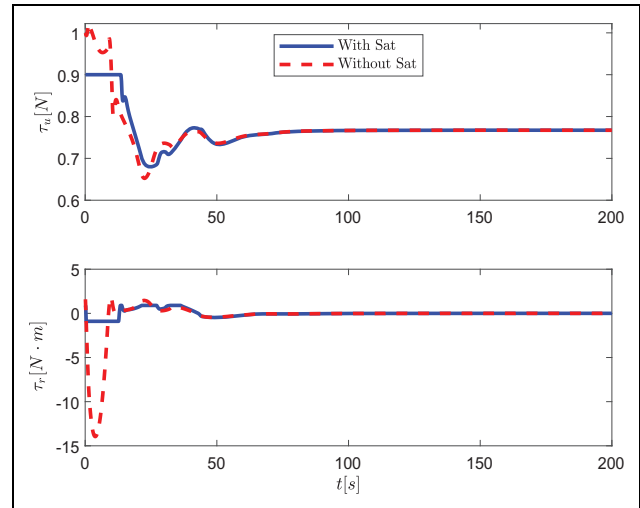


**Figure 18.** The control laws  $\tau_u$  and  $\tau_r$ .

Figure 13. And then, Figure 14 shows the velocity trending  $\dot{\theta}$  of virtual target. The estimation of unknown dynamics and system states are described in Figures 15 to 17. Finally, control inputs are depicted in Figure 18, which demonstrated that the presented scheme can provide effective anti-windup in the presence of saturation constraint. It is worth noting that the real control inputs will damage actuators in the same setting conditions and design parameters without anti-windup.

## Conclusion

This article develops a novel FPANN scheme for path following of USVs with unknown dynamics and input saturation. The presented FPLOS guidance laws, control laws, and auxiliary system in this scheme ensure USVs effective converging to and following the predefined path. It is shown via Lyapunov stability theory that the closed-loop

system is SGUUB. Simulation results demonstrate the effectiveness and performance of the presented FPANN scheme. In addition, there are many open problems for future investigation, such as external disturbances, dead-zone input nonlinearity, state constraint (e.g. yaw rate), and fault tolerant, which will be the focus of our further study.


### Declaration of conflicting interests

The author(s) declared no potential conflicts of interest with respect to the research, authorship, and/or publication of this article.

### Funding

The author(s) disclosed receipt of following financial support for the research, authorship, and/or publication of this article: This work was supported by the National Natural Science Foundation of China under Grant 51879027, 51579024, 6137114, and 51809028 and in partly by the Fundamental Research Funds for the Central Universities under grant 3132016311 and 3132018154.

### ORCID iD

Yalei Yu  <http://orcid.org/0000-0002-4916-1548>

### References

1. Fossen TI. *Handbook of marine craft hydrodynamics and motion control*. Trondheim, Norway: John Wiley & Sons, 2011.
2. Liu L, Wang D, and Peng Z. ESO-based line-of-sight guidance law for path following of underactuated marine surface vehicles with exact sideslip compensation. *IEEE J Ocean Eng* 2017; 42(2): 477–487.
3. Wang N, Sun Z, Zheng Z, et al. Finite-time sideslip observer-based adaptive fuzzy path-following control of underactuated marine vehicles with time-varying large sideslip. *Int J Fuzzy Syst* 2017: 1–12.
4. Chen G, Yang W, Fu-chun S, et al. Survey for motion control of underactuated surface vessels. *Control Decis* 2009; 24(3): 321–328. DOI: DOI10.13195/j.cd.2009.03.3.guoch. 012.
5. Miao J, Wang S, Tomovic MM, et al. Compound line-of-sight nonlinear path following control of underactuated marine vehicles exposed to wind, waves, and ocean currents. *Nonlin Dynam* 2017; 89(4): 2441–2459.
6. Zheng Z, Sun L, and Xie L. Error-constrained LOS path following of a surface vessel with actuator saturation and faults. *IEEE Trans Syst Man Cybern* 2017; 48(10): 1794–1805.
7. Wang N, Sun Z, Yin J, et al. Finite-time observer based guidance and control of underactuated surface vehicles with unknown sideslip angles and disturbances. *IEEE Access* 2018; 6: 14059–14070.
8. Skjetne R, Fossen TI, and Kokotovic PV. Robust output maneuvering for a class of nonlinear systems. *Automatica* 2004; 40(3): 373–383.
9. Fossen TI, Pettersen KY, and Galeazzi R. Line-of-sight path following for Dubins paths with adaptive sideslip compensation of drift forces. *IEEE Trans Control Syst Technol* 2015; 23(2): 820–827.
10. Lekkas AM and Fossen TI. Integral los path following for curved paths based on a monotone cubic hermite spline parametrization. *IEEE Trans Control Syst Technol* 2014; 22(6): 2287–2301.
11. Fossen TI and Lekkas AM. Direct and indirect adaptive integral line-of-sight path-following controllers for marine craft exposed to ocean currents. *Int J Adapt Control Signal Proc* 2017; 31(4): 445–463.
12. Zheng Z and Sun L. Path following control for marine surface vessel with uncertainties and input saturation. *Neurocomputing* 2016; 177(C): 158–167.
13. Liu L, Wang D, Peng Z, et al. Predictor-based los guidance law for path following of underactuated marine surface vehicles with sideslip compensation. *Ocean Eng* 2016; 124: 340–348.
14. Khaled N and Chalhoub NG. A self-tuning guidance and control system for marine surface vessels. *Nonlin Dynam* 2013; 73(1–2): 897–906.
15. Jin X. Fault tolerant finite-time leader–follower formation control for autonomous surface vessels with LOS range and angle constraints. *Automatica* 2016; 68: 228–236.
16. Yan Z, Yu H, Zhang W, et al. Globally finite-time stable tracking control of underactuated UUVs. *Ocean Eng* 2015; 107: 132–146.
17. Wang N, Lv S, Zhang W, et al. Finite-time observer based accurate tracking control of a marine vehicle with complex unknowns. *Ocean Eng* 2017; 145: 406–415.
18. Qiao L and Zhang W. Double-loop integral terminal sliding mode tracking control for UUVs with adaptive dynamic compensation of uncertainties and disturbances. *IEEE J Ocean Eng* 2018; 2018: 1–25.
19. Jayasiri A, Nandan A, Imtiaz S, et al. Dynamic positioning of vessels using a UKF-based observer and an NMPC-based controller. *IEEE Trans Auto Sci Eng* 2017; 14(4): 1778–1785.
20. Liu H, Wu Y, Sun F, et al. Weakly paired multimodal fusion for object recognition. *IEEE Transact Auto Sci Eng* 2018; 15(2): 784–795.
21. Yin Z, He W, Yang C, et al. Adaptive control of a marine vessel based on reinforcement learning. *Neurocomputing* 2018.
22. Zhang G, Zhang X, and Zheng Y. Adaptive neural path following control for underactuated ships in fields of marine practice. *Ocean Eng* 2015; 104: 558–567.
23. Chen M, Ge SS, and How BVE. Robust adaptive neural network control for a class of uncertain MIMO nonlinear systems with input nonlinearities. *IEEE Trans Neural Netw* 2010; 21(5): 796–812.
24. Shojaei K. Neural adaptive robust control of underactuated marine surface vehicles with input saturation. *Appl Ocean Res* 2015; 53: 267–278.
25. Gao YF, Sun XM, Wen C, et al. Observer-based adaptive NN control for a class of uncertain nonlinear systems with non-symmetric input saturation. *IEEE Trans Neural Netw Learn Syst* 2017; 28(7): 1520–1530.

26. Liu C, Zou ZJ, and Li TS. Path following of underactuated surface vessels with fin roll reduction based on neural network and hierarchical sliding mode technique. *Neural Comput Appl* 2015; 26(7): 1525–1535.
27. He W, Yin Z, and Sun C. Adaptive neural network control of a marine vessel with constraints using the asymmetric barrier Lyapunov function. *IEEE Trans Cybern* 2017; 47(7): 1641–1651.
28. Liu L, Wang D, and Peng Z. Path following of marine surface vehicles with dynamical uncertainty and time-varying ocean disturbances. *Neurocomputing* 2016; 173(pt 3): 799–808.
29. Yang YS and Wang XF. Adaptive  $H_\infty$  tracking control for a class of uncertain nonlinear systems using radial-basis-function neural networks. *Neurocomputing* 2007; 70(4–6): 932–941.
30. Li TS, Wang D, Feng G, et al. A DSC approach to robust adaptive NN tracking control for strict-feedback nonlinear systems. *IEEE Trans Syst Man Cybern b* 2010; 40(3): 915–927.
31. Miao B and Li T. A novel neural network-based adaptive control for a class of uncertain nonlinear systems in strict feedback form. *Nonlin Dynam* 2015; 79(2): 1005–1013.
32. Yan Z, Wang M, and Xu J. Global adaptive neural network control of underactuated autonomous underwater vehicles with parametric modeling uncertainty. *Asian J Control* 2019; 21(4): 1–13.
33. Bu X, Wu X, Huang J, et al. Minimal-learning-parameter based simplified adaptive neural back-stepping control of flexible air-breathing hypersonic vehicles without virtual controllers. *Neurocomputing* 2016; 175(PA): 816–825.
34. Yang Y and Ren J. Adaptive fuzzy robust tracking controller design via small gain approach and its application. *IEEE Trans Fuzzy Syst* 2003; 11(6): 783–795.
35. Chen B, Liu X, Liu K, et al. Direct adaptive fuzzy control of nonlinear strict-feedback systems. *Automatica* 2009; 45(6): 1530–1535.
36. Song Y, Huang X, and Wen C. Tracking control for a class of unknown nonsquare MIMO nonaffine systems: a deeprooted information based robust adaptive approach. *IEEE Trans Autom Control* 2016; 61(10): 3227–3233.
37. Wang N, Sun JC, Han M, et al. Adaptive approximation based regulation control for a class of uncertain nonlinear systems without feedback linearizability. *IEEE Trans Neural Netw Learn Syst* 2017; 29(8): 3747–3760.
38. Chen M, Ge SS, and Choo YS. Neural network tracking control of ocean surface vessels with input saturation. In: *ICAL'09. IEEE international conference on automation and logistics, 2009, Shenyang, China, 5–7 August 2009*, pp. 85–89. IEEE.
39. Zheng Z and Feroskhan M. Path following of a surface vessel with prescribed performance in the presence of input saturation and external disturbances. *IEEE/ASME Trans Mech* 2017; 22(6): 2564–2575.
40. Du J, Hu X, Krstic M, et al. Robust dynamic positioning of ships with disturbances under input saturation. *Automatica* 2016; 73: 207–214.
41. Cui R, Zhang X, and Cui D. Adaptive sliding-mode attitude control for autonomous underwater vehicles with input nonlinearities. *Ocean Eng* 2016; 123: 45–54.
42. Li T, Li R, and Li J. Decentralized adaptive neural control of nonlinear interconnected large-scale systems with unknown time delays and input saturation. *Neurocomputing* 2011; 74(14–15): 2277–2283.
43. Harmouche M, Laghrouche S, and Chitour Y. Global tracking for underactuated ships with bounded feedback controllers. *Int J Control* 2014; 87(10): 2035–2043.
44. Wang N, Su SF, Han M, et al. Backpropagating constraints based trajectory tracking control of a quadrotor with constrained actuator dynamics and complex unknowns. *IEEE Trans Syst Man Cybern Syst* 2018; 2018: 1–16.
45. Chen M and Ge SS. Direct adaptive neural control for a class of uncertain nonaffine nonlinear systems based on disturbance observer. *IEEE Trans Cybern* 2013; 43(4): 1213–1225.
46. Cheng L, Hou ZG, and Tan M. Adaptive neural network tracking control for manipulators with uncertain kinematics, dynamics and actuator model. *Automatica* 2009; 45(10): 2312–2318.
47. Park BS, Kwon JW, and Kim H. Neural network-based output feedback control for reference tracking of underactuated surface vessels. *Automatica* 2017; 77: 353–359.
48. Do KD and Pan J. Global tracking control of underactuated ships with nonzero off-diagonal terms in their system matrices. *Automatica* 2005; 41(1): 87–95.
49. Hardy GH, Littlewood JE, and Polya G. *Inequalities. Reprint of the 1952 edition*. Cambridge: Cambridge mathematical library, 1988.
50. Yu S, Yu X, Shirinzadeh B, et al. Continuous finite-time control for robotic manipulators with terminal sliding mode. *Automatica* 2005; 41(11): 1957–1964.
51. Bhat SP and Bernstein DS. Finite-time stability of continuous autonomous systems. *SIAM J Control Optim* 2000; 38(3): 751–766.
52. Wang N, Qian C, Sun JC, et al. Adaptive robust finite-time trajectory tracking control of fully actuated marine surface vehicles. *IEEE Trans Control Syst Technol* 2016; 24(4): 1454–1462.
53. Krstic M, Kanellakopoulos I, Kokotovic PV, et al. *Nonlinear and adaptive control design*, vol. 222. New York: Wiley, 1995.
54. Lewis FL, Dawson D, and Abdallah CT. *Control of Robot Manipulators*. Croatia: Prentice Hall PTR, 1993.
55. Khalil HK. *Nonlinear Systems*. 3rd ed. NJ, USA: Prentice-Hall, 2002.
56. Van Amerongen J. Adaptive steering of ships: a model reference approach. *Automatica* 1984; 20(1): 3–14.
57. Hermosilla C, Vinter R, and Zidani H. Hamilton–Jacobi–Bellman equations for optimal control processes with convex state constraints. *Syst Control Lett* 2017; 109: 30–36.
58. Lefeber E, Pettersen KY, and Nijmeijer H. Tracking control of an underactuated ship. *IEEE Trans Control Syst Technol* 2003; 11(1): 52–61.